


 Cite this: *Lab Chip*, 2021, 21, 2265

## Rotational scan digital LAMP for accurate quantitation of nucleic acids†

 Mengcheng Jiang,<sup>ab</sup> Peiyu Liao,<sup>ab</sup> Yue Sun,<sup>bc</sup> Xinyang Shao,<sup>bc</sup> Zitian Chen,<sup>ab</sup> Peng Fei,<sup>id</sup> Jianbin Wang<sup>e</sup> and Yanyi Huang<sup>id</sup>\*<sup>abcf</sup>g

Digital quantitation of nucleic acids is precise and sensitive because of its molecular-level resolution. However, only several quantitation formats are common, especially pertaining to how one obtains digital signals from multiple droplets. Here we present rotational scan digital loop-mediated amplification, termed RS-dLAMP. Droplets generated by centrifugation undergo isothermal loop-mediated amplification (LAMP), and self-tile by gravitation into a tubular space between two coaxial cylinders, which are then rotated and scanned to acquire droplet fluorescence signals. RS-dLAMP is quantitatively comparable to commercial digital PCR, yet has higher throughput. Moreover, by sealing the sample throughout analysis, RS-dLAMP eliminates contamination, facilitating point-of-care diagnosis and other applications.

 Received 14th February 2021,  
 Accepted 19th April 2021

DOI: 10.1039/d1lc00114k

[rsc.li/loc](https://rsc.li/loc)

### Introduction

Recent developments in digital quantification of nucleic acids have pushed the limit of DNA and RNA detection to the single-molecule level as a result of the ‘divide and conquer’ strategy.<sup>1</sup> After isolating single nucleic acid fragments in separate compartments, digital quantitation is realized by counting the positive compartments.<sup>2–4</sup> Standard curves are not needed and there is less amplification bias among template molecules. Digital PCR is an emerging technology for high-sensitivity and high-accuracy detection.<sup>4–7</sup>

A major technical milestone in digital PCR development was the introduction of microfluidics to perform compartmentalization; for example, solid micro-chambers<sup>8–11</sup> or water-in-oil droplets.<sup>12–15</sup> Compartmentalization brought digital counting to laboratory experiments and completely changed how researchers quantify DNA or RNA molecules, with accuracies much higher than conventional quantitative real-time PCR.<sup>16</sup>

A complete digital quantitation system for nucleic acids contains three major parts: partitioning, amplification, and counting. Recently, droplet-based partitioning has gained popularity compared with solid-chamber-based strategies because of the comparatively lower cost and better flexibility of droplet microfluidics.<sup>17</sup> Regarding amplification, PCR remains the most favored option, yet isothermal chemistries are becoming increasingly popular and offer additional options.<sup>18–20</sup> The obvious strength that underlies isothermal amplification is elimination of thermal cyclers, which leads to lower costs, easier operation, and improved monitoring. These advantages facilitate point-of-care testing and resource-limited applications.<sup>21–26</sup>

Innovation in counting, however, remains limited. Counting can be performed in series<sup>27–29</sup> or parallel.<sup>30–33</sup> The former approach is more popular but is time-consuming and costly. Imaging-based signal acquisition takes advantage of parallel counting but is challenging to couple with centrifuge-tube-based PCR. Recently, we reported a three-dimensional in-tube counting strategy: light-sheet fluorescence imaging and an optically clear emulsion system to eliminate material loss and cross-contamination.<sup>34</sup> However, the additive we used for adjusting the refractive index of the droplets may not be compatible with all biochemical reactions. To optimize digital nucleic acid quantification, one should minimize costly and complicated components or processes. We conducted a simple rotational scan on a thin layer of emulsion with isothermal loop-mediated amplification (LAMP), to digitally count target nucleic acids. With this rotational scan digital LAMP (RS-dLAMP) approach, water-in-oil droplets are sealed after droplet generation. Hence, we completely eliminated

<sup>a</sup> Materials Science and Engineering, College of Engineering, Peking University, Beijing, China. E-mail: [yanyi@pku.edu.cn](mailto:yanyi@pku.edu.cn)

<sup>b</sup> Biomedical Pioneering Innovation Center (BIOPIC) and Beijing Advanced Innovation Center for Genomics (ICG), Peking University, Beijing, China

<sup>c</sup> Peking-Tsinghua Center for Life Sciences, Peking University, Beijing, China

<sup>d</sup> School of Optical and Electronic Information-Wuhan National Laboratory for Optoelectronics, Huazhong University of Science and Technology, Wuhan, China

<sup>e</sup> School of Life Sciences, Beijing Advanced Innovation Center for Structural Biology, Beijing, China

<sup>f</sup> College of Chemistry and Molecular Engineering, and, Beijing National Laboratory for Molecular Sciences, Peking University, Beijing, China

<sup>g</sup> Institute for Cell Analysis, Shenzhen Bay Laboratory, Shenzhen, China

† Electronic supplementary information (ESI) available. See DOI: 10.1039/d1lc00114k

contamination while no microfluidic component was used in the whole process. This minimalism method may offer new insight on cost-efficient and facile nucleic acid quantitation for biotechnological applications that use droplets as reactors.

## Results and discussion

### Experimental procedure and setup design

Most droplet generation approaches are based on a microfluidic chip, through which droplets are first produced then commonly transferred into micro-centrifuge tubes for subsequent reactions. Instead, we used our previously reported micro-channel array (MiCA) to generate monodisperse droplets into the tubes directly, facilitating minimal sample loss and complete bulk-to-droplet conversion (Fig. 1a).<sup>34–36</sup> Under centrifugal force, the aqueous LAMP reaction mix was driven through the micro-capillary array, pinched into droplets at the liquid–air interface, and then submerged into the underlying emulsion oil.

Centrifugation requires  $\sim 3$  min and multiple samples can be processed simultaneously. Upon droplet formation, we then inserted a polycarbonate (PC) rod—attached to the lid—into the tube and closed the lid. The diameter of the rod was 300  $\mu\text{m}$  smaller than the inner diameter of the tube, leaving a 150  $\mu\text{m}$  thick tubular space between the rod and tube inner surface. We incubated the tubes in a metal bath at 65  $^{\circ}\text{C}$  for 60 min to perform LAMP (Fig. 1b). Then we placed the tubes

upside down and waited for 20 min, over which time the droplets gradually sank and slid into the gap space (Fig. 1c). Amplification was indicated through fluorescence SYTO-9 nucleic acid stain. To capture the fluorescence signal in the droplets, we cast a line-shaped laser beam on the tube's cylindrical surface for excitation and rotated the tube to scan the entire emulsion (Fig. 1d). Typically, we acquired 800 frames within 16 s for each sample (Fig. 1e). Instead of simple repositioning tiling, we developed a time delay integration algorithm to reconstruct the panorama images from corresponding small frames. For excitation, we reshaped and expanded a 488 nm laser into a line-shaped beam using a combination of two cylindrical lenses (Fig. 1f). Epifluorescence imaging was as follows: two band-pass filters and a dichroic mirror to eliminate background light, and a scientific complementary metal oxide semiconductor (sCMOS) camera to capture high-frame-rate images.

### Performance of RS-dLAMP

We designed the rod to fit into micro-centrifuge tubes and took advantage of the lid flange to attach the rod (Fig. 2a). We used palmitate oil as the continuous (oil) phase and silicone copolymer such as ABIL EM180 as surfactant in the disperse (aqueous) phase. A previous study showed that such oil–surfactant combinations have sufficient thermal stability for 65  $^{\circ}\text{C}$  LAMP.<sup>37</sup> The emulsion was opaque (Fig. 2b) and could not be imaged in the tube without opening the lid. We

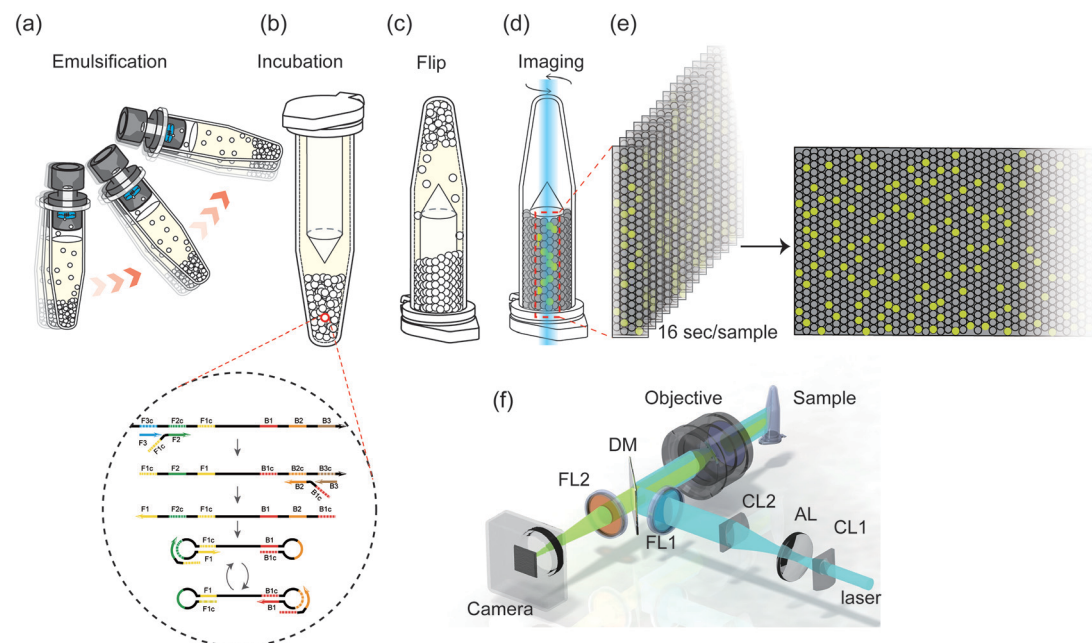


**Fig. 1** Schematic of rotational scan digital loop-mediated amplification (RS-dLAMP). (a) Monodisperse droplets are first generated under centrifugation using a micro-capillary array (MiCA). (b) A polycarbonate (PC) rod is inserted into the emulsion oil and the entire tube is incubated at 65  $^{\circ}\text{C}$  to perform LAMP. (c) When the reaction is finished, the sealed tube is flipped; the droplets fall into the gap between the rod's cylindrical wall and form an even layer ( $\sim 150$   $\mu\text{m}$ ) of packed droplets. (d) To count the droplets, we used a line-shaped light beam for excitation, and rotated the tube to scan the entire emulsion for fluorescence imaging. (e) A stack of small fluorescence image is captured by a camera and stitched into a panorama. (f) The light path. A 488 nm laser is reshaped and expanded into a line-shaped beam by two cylindrical lenses (CL1 and CL2) and an aspherical lens (AL). An excitation filter (FL1), an emission filter (FL2), a dichroic mirror (DM), and a wide-field objective are used for epifluorescence imaging.

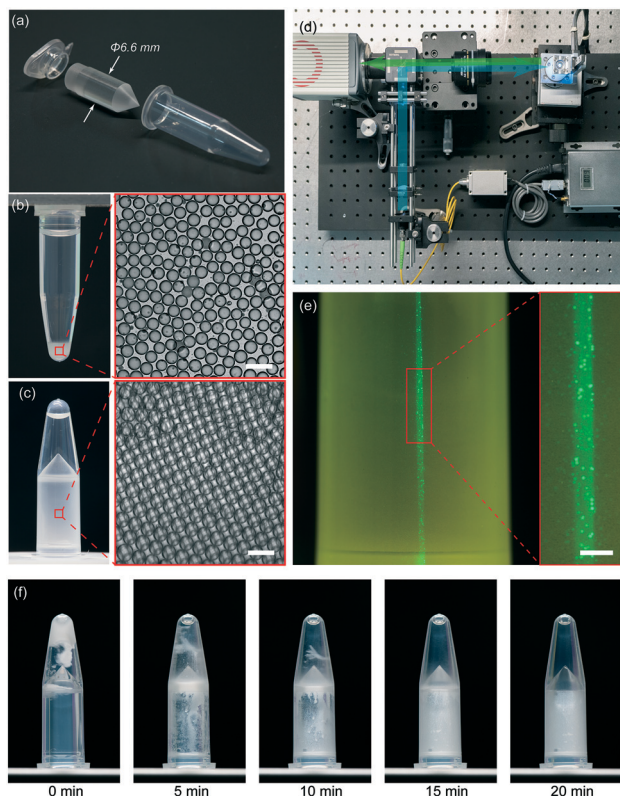


**Fig. 2** Device and imaging system of RS-dLAMP. (a) We machined the PC rod and then attached it to the lid. (b) Droplets are generated under centrifugation using a MiCA. Scale bar: 100  $\mu\text{m}$ . (c) After inserting the rod insertion and flipping the tube, a cylindrical layer of droplets formed between the rod and inner surface of the centrifuge tube, and the droplets were packed in this space. Scale bar: 100  $\mu\text{m}$ . (d) Rotational scan setup. Droplets in the tube are excited by a 488 nm laser; a scientific complementary metal oxide semiconductor (sCMOS) camera captures emitted light. (e) Fluorescent droplets under line-shaped laser excitation. Scale bar: 500  $\mu\text{m}$ . (f) Packing process of sinking droplets after flipping the tube.

carefully designed the diameter of the rod to have a  $\sim 150$   $\mu\text{m}$  gap between the rod and tube inner surface. Droplets sank into the gap and packed together (Fig. 2c). The droplets were mechanically stable and remained intact and monodisperse. The rotational scan system (Fig. 2d) was compact and constructed on a  $30 \times 60$  cm optical bread board. Unlike most epifluorescence imaging designs that use planar illumination, our design increased the excitation intensity using a line-shaped laser beam (Fig. 2e). Consequently, the scanning speed could be increased.

We then evaluated the performance of RS-dLAMP. We designed a primer set consisting of six oligonucleotides (FIP/BIP, F3/B3, and F1c/B1c) that targeted M13mp18 bacteriophage single-stranded DNA (Fig. 1b). We added intercalating dye SYTO-9 to the reaction mixture, which turns a droplet fluorescent if there is an increase in double-strand DNA concentration over the course of isothermal amplification.

The oil phase consisted of 93% (v/v) isopropyl palmitate (Sigma-Aldrich) and 7% (v/v) ABIL EM180 (Evonik), with a

density of  $0.85 \text{ g cm}^{-3}$  and a viscosity of 12 cSt. The relatively low viscosity prevented aqueous droplets from coalescing and breaking.<sup>37</sup> Moreover, the oil has lower solubility to SYTO-9 dye than mineral oil. SYTO-9 diffuses into mineral oil at high temperatures, causing undesired fluorescence background in the emulsion. Emulsion generation was efficient, requiring  $\sim 3$  min, providing  $\sim 554\,000$  droplets with an average diameter of 41  $\mu\text{m}$  using MiCA for each reaction. The droplets then packed into the 150  $\mu\text{m}$ -thick cylindrical layer within 20 min by gravity (Fig. 2f), requiring minimal hands-on operation.

We then mounted the flipped tube onto a motorized rotation stage for imaging. The spinning speed was  $25^\circ \text{ s}^{-1}$ . It typically required  $\sim 16$  s to capture the image of a complete tube with frame rate of 50 fps (800 frames in total). Each frame was  $48 \times 2048$  pixels. We streamlined image processing to accurately count positive droplets. The high frame rate of imaging ensured that we observed each droplet in six successive frames (Fig. 3a). One simple stitching strategy is to crop the central part of each frame and stitch the cropped images into a composite (Fig. 3b). However, this could introduce a stripe pattern—originating from the uneven illumination—in the stitched image. Instead, we aligned fluorescent signals of the same droplet in several frames, and then averaged the pixel intensity to obtain a composite image with lower noise (Fig. 3c). Then, we further corrected the image background unevenness (Fig. 3d). We used a white top-hat transform to eliminate the background intensity (Fig. 3e) and hence increase the signal-to-noise ratio (Fig. 3f). Positive droplets were clearly brighter than the surrounding negative droplets, facilitating identification (Fig. 3g). We corrected the number of positive droplets by Poisson distribution using a previously described algorithm.<sup>35</sup>

To test the performance of RS-dLAMP in absolute quantification of nucleic acids, we diluted template DNA into seven concentration sets ( $\sim 1$  to  $\sim 1000 \text{ cp } \mu\text{L}^{-1}$ ), each with five replicates. The unrolled surface of the cylindrical rod is sufficiently large for detection of fluorescent positive droplets with a dynamic range across five orders of magnitude. For comparison and validation, we also designed PCR primers along with a TaqMan probe for a commercial digital PCR platform (Bio-Rad QX200 ddPCR) to quantify the same samples (Fig. 4a). RS-dLAMP and digital PCR results were highly concordant, although the positive counts obtained from QX200 was lower than those from RS-dLAMP (Fig. 4b). The serial counting process, *e.g.* the Bio-Rad QX200 ddPCR instrument, will typically contain  $\sim 30\%$  sample loss due to the dead volume and the stabilization period of the microfluidic operation. Such loss has to be corrected by subsequent data processing, while nearly all droplets are scanned in RS-dLAMP process. We also designed another set of primers targeting Lambda phage DNA, performed gel electrophoresis as well as RS-dLAMP to cross validate the specificity of LAMP (Fig. S3 and S4<sup>†</sup>). The rotational scan was efficient and required no more than 16 s to count a sample, whereas serial counting usually required several minutes.

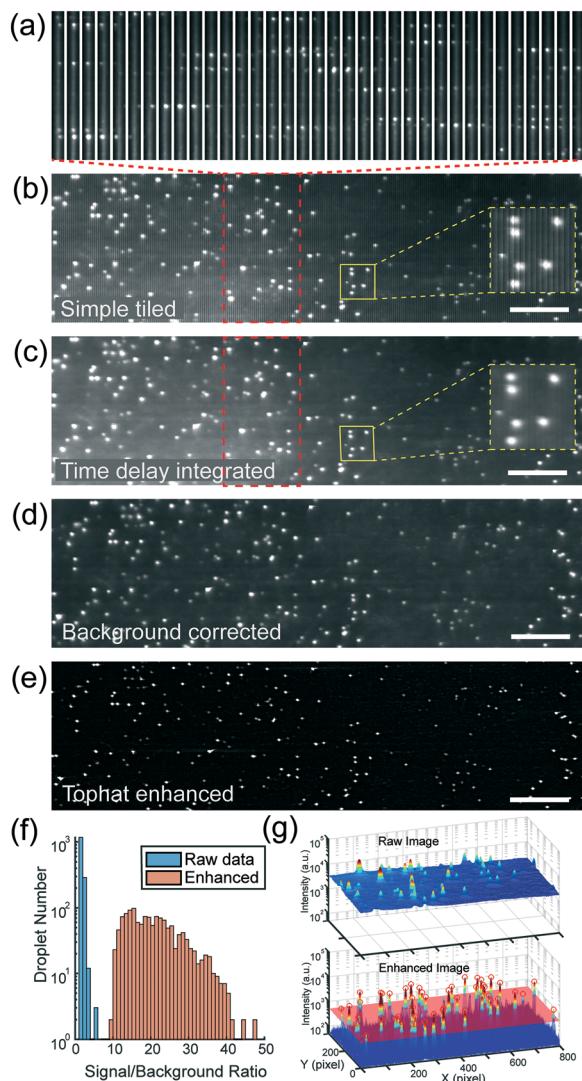


**Fig. 3** Image processing and counting of fluorescent droplets in RS-dLAMP. (a) Original images successively captured during rotational spin of the sample. We captured each droplet in six frames. (b) Simple stitching of captured frames caused vertical stripes. (c) Time delay integration generated a stitched image with a smooth background. (d) Corrected background unevenness. (e) We used a white top-hat transform to improve the signal-to-noise ratio. (f and g) The signal-to-noise ratio of the droplets improved after image enhancement. Scale bars: 1 mm.

Furthermore, compared with serial counting, rotational scanning did not require post-amplification droplets to be transferred out of the micro-centrifuge tubes; thus, we completely eliminated cross-sample contamination. For biomedical quantification methods with single-copy sensitivity, lid-opening is often to be avoided. The *in situ* counting scheme of RS-dLAMP is also a more precise way for digital amplification because it does not exhibit errors from sub-sampling, offering a lower limit of detection analogously to CLEAR-dPCR.<sup>34</sup>

Digital quantification of nucleic acids is an established topic; researchers have proposed many approaches, and

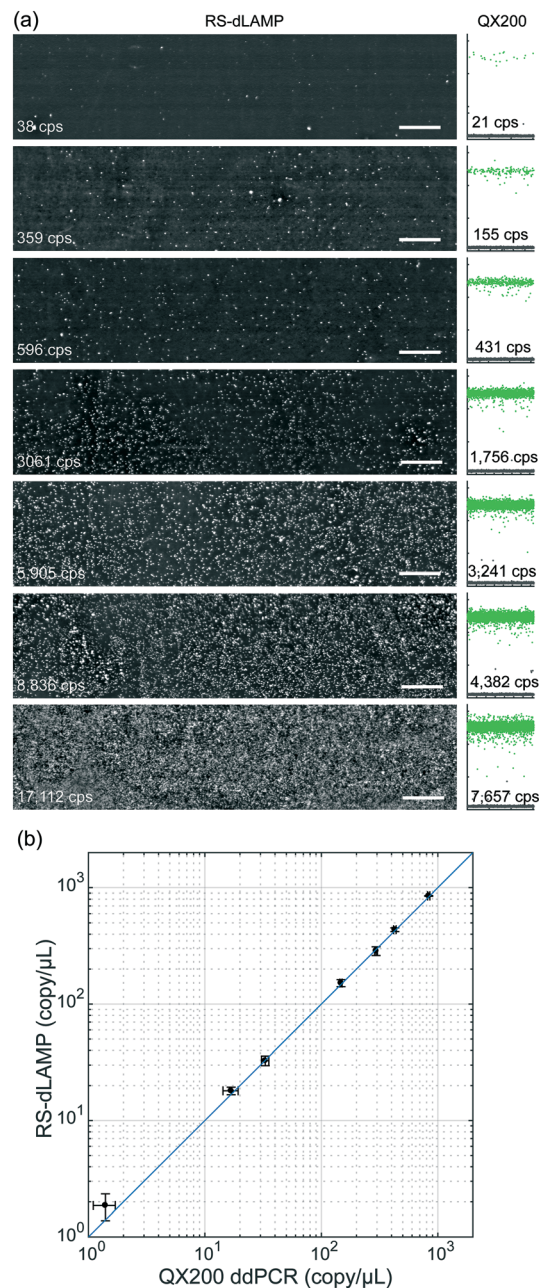


**Fig. 4** Counting fluorescent droplets in RS-dLAMP. (a) Representative results of RS-dLAMP, shown as stitched images with positive counts determined by image analysis. Scale bars: 2 mm. We tested the same sets of samples using digital PCR (Bio-Rad QX200). (b) Concordance of RS-dLAMP and digital PCR quantification results; error bars are the standard deviations.

digital PCR is an active area of research. In this study, we addressed two major challenges that hinder applications of digital quantification. First, digital counting should be straightforward; no sample transfer that may cause cross-contamination.<sup>38</sup> In our previous work we designed an optically clear emulsion system that meets this experimental requirement when the two phases of the emulsion are refractive-index-matched. Although we discovered that certain additives that increase the refractive index of the reaction

buffer would not inhibit PCR,<sup>34</sup> such additives affect the reaction kinetics and hence necessitated adjustment of the reaction conditions. Rotational scanning can work well with normal emulsions without extra additives to match the refractive indices, increasing the compatibility to various amplification chemistries, such as many isothermal approaches. Second, isothermal amplification is probably the best fit for chip-free droplet generation and lid-closed *in situ* counting.<sup>24,39</sup> A combination of centrifugation, isothermal amplification, and a more-straightforward imaging scheme will be a plausible solution for many clinical applications.

There is still room for further improvement. Since the mass production of rod inserts can be easily accomplished by injection moulding, the supply cost per sample is significantly reduced compared to other chip-based digital quantification methods using microfluidic channels or micro well arrays. The current instrumentation takes only a small layout with acceptable portability, the further reduction of hardware cost and dimension is still promising. For example, the imaging setup can be re-designed to use inexpensive and mass-produced devices—for example, smart-phones with cameras—to greatly reduce the technical difficulties of digital quantification methodologies.<sup>40–42</sup> One can also replace the laser—an expensive option that is unnecessary to generate a linear beam at this scale—with much cheaper light-emitting diode light sources. In addition, the image processing only requires minimal computing resource which can be done on a common laptop even on smartphones if necessary.

Manual sample loading and unloading can be easily automated to minimize the labour and scale up to higher throughput in a clinical working environment. Furthermore, our system is compatible with fluorocarbon oil, with a density higher than the aqueous phase; there would be no need to flip the tube, such that droplets in the fluorocarbon oil can be scanned while the tube is upright. Being cost-efficient and user-friendly, RS-dLAMP will better serve biomedical researchers and precision medicine.

## Conclusions

We report a digital LAMP technique, primarily focusing on counting droplets, to enhance *in situ* digital quantification of nucleic acids. RS-dLAMP has three major advantages. First, it takes advantage of the MiCA droplet generation method, which uses a rod-insert to make a cylindrical space inside the micro-centrifuge tube for droplets to form an even layer under gravity. We did not use chip-based microfluidic components and it reduces the cost and operation complexity of this approach. Second, our method is contamination-free and thus ideal for pathogen detection and other clinical applications that repeatedly amplify the same specific region. Last but not least, the use of line scan technology greatly improves imaging speed, it only takes 16 s to scan one sample while several minutes are typically needed for serial counting. RS-dLAMP is inexpensive, facile, and reliable.

Researchers can integrate it into various experimental designs.

## Experimental

### Materials

Table S1† lists LAMP primers, synthesized by Sangon Biotech (Shanghai) Co., Ltd. M13mp18 single-stranded DNA (NEB catalog#: N4040S) was diluted into various concentrations as template solutions, and a 2× premix was prepared in accordance with Table S2.† For each template concentration, 10 μL template solution and 40 μL nuclease-free water was added to 50 μL premix. Then, the 100 μL reaction mixture was loaded into five MiCA tubes, 20 μL each, and spun at 15 000 rcf for 3 min in an Eppendorf 5430R centrifuge. The resulting emulsion droplets were first kept static for 5 min to stabilize the droplets. Next, PC fillers were inserted into the tubes and heated to 65 °C, and incubated for 1 h to complete LAMP. After incubation, the tubes were flipped upside down, waiting 20 min to let the droplets slide into the gap and pack into a thin layer. Each tube was then mounted onto the rotation stage of the scanning system to acquire fluorescence images.

The final concentration of diluted template was validated by Bio-Rad QX200 digital PCR platform. We designed PCR primers and Taqman probes for absolute quantitation; Table S3† lists the oligonucleotide sequences. Samples used in RS-dLAMP were quantified by Bio-Rad QX200 ddPCR in accordance with Table S4.† One hundred microliters of reaction mixture of each template concentration was prepared and separated into five parallel samples—20 μL each—for droplet generation, PCR amplification, and digital counting.

### Design of rod-insert

The rod insert was made by CNC machining of polycarbonate rods, as per the dimensions shown in Fig. S1.† The cylindrical surface was mirror-polished for improved light transmission. Six claws at the upper and lower position of the imaging surface kept the space between the rod and inner surface of the centrifuge tube uniform and kept the rod's axis in accordance with that of the centrifuge tube.

### Imaging setup

For sample illumination and imaging, a fiber-coupled 488 nm laser was used as the excitation source. The laser was first collimated into a Gaussian beam, diameter ~3.3 mm, using a collimator. Then an aspherical lens ( $f = 8$  mm) and two cylindrical lenses ( $f = 12.7$  mm, 50 mm) were used to transform the beam into an elliptical shape ~13 mm height and ~0.2 mm wide to excite a linear area on the tube. A widefield objective (Nikon AZ Plan Apo 1×) and an sCMOS camera (Hamamatsu ORCA Flash 4.0 V2) was used for fluorescent imaging (Fig. 2d). Because the surface of the centrifuge tube was cylindrical and the depth of field of the

objective lens was limited, only a narrow linear area ( $\sim 10$  mm height,  $\sim 0.2$  mm wide) was in focus for imaging.

To acquire high-quality images of the cylindrical surface of the centrifuge tubes, it is critical to keep the tubes coaxial with the rotational axis. A 3D printed holder was used to fit the cap, and a ball bearing (MR106ZZ bearing, NSK Inc.) fit the bottom of the tube. The cap holder was mounted on the rotational stage; an adapter held the ball bearing and was mounted on a slide unit (ML9C1S1, IKO Inc.). The slide unit can move vertically on a linear rail to render sample switching convenient. The other essential requirement for the system is a stable rotation speed when scanning. An RCP2 rotary actuator from IAI Inc. showed excellent performance in our experiments. Fig. S2† shows the assembly details of the rotation mechanics.

### Image processing

The raw data were 800 sequential images,  $48 \times 2048$  pixels each. The position shift between two adjacent images was 8 pixels, which means a droplet's signal would appear on six images. We aligned adjacent images by a position shift depending on the rotation speed. Then, the aligned images were averaged to obtain a panorama image with a higher signal-to-noise ratio, while eliminating the vertical stripes that would be caused by using a simple frame-tilling algorithm. The panorama image's background unevenness was corrected by multiplying the correction profile, which was acquired by Gaussian filtering of the original panorama with a standard deviation of 100. Morphological white top-hat was used to enhance the fluorescent droplet signal. Droplet positions and intensities were then acquired by determining the local maxima of the enhanced panorama image. An intensity threshold was set according to the distribution of the local maxima intensities to filter out background noise. The MATLAB codes of image processing and counting are available at [https://github.com/MengchengJ/RS-dLAMP\\_counting](https://github.com/MengchengJ/RS-dLAMP_counting).

### Author contributions

Y. H., P. L., M. J. and J. W. conceived the idea and designed the study. M. J. designed the optical scanning system and image processing algorithm. Y. S. optimized LAMP in droplets. X. S., Z. C. and P. F. aided in experimental design and contributed to the discussion. M. J., P. L., and Y. H. wrote the paper. All authors commented on the manuscript.

### Funding

This work was supported by the National Key R&D Program of China (2018YFA0108100), National Natural Science Foundation of China (21927802 and 22050002), Beijing Advanced Innovation Center for Genomics, and Shenzhen Bay Laboratory.

### Conflicts of interest

There are no conflicts to declare.

### Notes and references

- 1 P. Liao and Y. Huang, *Micromachines*, 2017, **8**, 231–237.
- 2 M. Baker, *Nat. Methods*, 2012, **9**, 541–544.
- 3 R. Sanders, J. F. Huggett, C. A. Bushell, S. Cowen, D. J. Scott and C. A. Foy, *Anal. Chem.*, 2011, **83**, 6474–6484.
- 4 P.-L. Quan, M. Sauzade and E. Brouzes, *Sensors*, 2018, **18**, 1271.
- 5 A. S. Devonshire, I. Honeyborne, A. Gutteridge, A. S. Whale, G. Nixon, P. Wilson, G. Jones, T. D. McHugh, C. A. Foy and J. F. Huggett, *Anal. Chem.*, 2015, **87**, 3706–3713.
- 6 Y. M. Lo, F. M. Lun, K. C. Chan, N. B. Tsui, K. C. Chong, T. K. Lau, T. Y. Leung, B. C. Zee, C. R. Cantor and R. W. Chiu, *Proc. Natl. Acad. Sci. U. S. A.*, 2007, **104**, 13116–13121.
- 7 E. A. Ottesen, J. W. Hong, S. R. Quake and J. R. Leadbetter, *Science*, 2006, **314**, 1464–1467.
- 8 K. A. Heyries, C. Tropini, M. Vaninsberghe, C. Doolin, O. I. Petriv, A. Singhal, K. Leung, C. B. Hughesman and C. L. Hansen, *Nat. Methods*, 2011, **8**, 649–651.
- 9 J. Wang, R. Ramakrishnan, Z. Tang, W. Fan, A. Kluge, A. Dowlati, R. C. Jones and M. C. P, *Clin. Chem.*, 2010, **56**, 623–632.
- 10 X. Bian, F. Jing, G. Li, X. Fan, C. Jia, H. Zhou, Q. Jin and J. Zhao, *Biosens. Bioelectron.*, 2015, **74**, 770–777.
- 11 Q. Zhu, L. Qiu, B. Yu, Y. Xu, Y. Gao, T. Pan, Q. Tian, Q. Song, W. Jin, Q. Jin and Y. Mu, *Lab Chip*, 2014, **14**, 1176–1185.
- 12 J. Chen, Z. Luo, L. Li, J. He, L. Li, J. Zhu, P. Wu and L. He, *Lab Chip*, 2018, **18**, 412–421.
- 13 Q. Zhong, S. Bhattacharya, S. Kotsopoulos, J. Olson, V. Taly, A. D. Griffiths, D. R. Link and J. W. Larson, *Lab Chip*, 2011, **11**, 2167–2168.
- 14 B. J. Hindson, K. D. Ness, D. A. Masquelier, P. Belgrader, N. J. Heredia, A. J. Makarewicz, I. J. Bright, M. Y. Lucero, A. L. Hiddessen, T. C. Legler, T. K. Kitano, M. R. Hodel, J. F. Petersen, P. W. Wyatt, E. R. Steenblock, P. H. Shah, L. J. Bousse, C. B. Troup, J. C. Mellen, D. K. Wittmann, N. G. Erndt, T. H. Cauley, R. T. Koehler, A. P. So, S. Dube, K. A. Rose, L. Montesclaros, S. Wang, D. P. Stumbo, S. P. Hodges, S. Romine, F. P. Milanovich, H. E. White, J. F. Regan, G. A. Karlin-Neumann, C. M. Hindson, S. Saxonov and B. W. Colston, *Anal. Chem.*, 2011, **83**, 8604–8610.
- 15 W. Zhang, N. Li, D. Koga, Y. Zhang, H. Zeng, H. Nakajima, J.-M. Lin and K. Uchiyama, *Anal. Chem.*, 2018, **90**(8), 5329–5334.
- 16 A. S. Whale, J. F. Huggett, S. Cowen, V. Speirs, J. Shaw, S. Ellison, C. A. Foy and D. J. Scott, *Nucleic Acids Res.*, 2012, **40**(11), e82.
- 17 L. Shang, Y. Cheng and Y. Zhao, *Chem. Rev.*, 2017, **117**(12), 7964–8040.
- 18 F. Schuler, C. Siber, S. Hin, S. Wadle, N. Paust, R. Zengerle and F. von Stetten, *Anal. Methods*, 2016, **8**, 2750–2755.

- 19 F. Schuler, F. Schwemmer, M. Trotter, S. Wadle, R. Zengerle, F. von Stetten and N. Paust, *Lab Chip*, 2015, **15**, 2759–2766.
- 20 L. Wan, T. Chen, J. Gao, C. Dong, A. H.-H. Wong, Y. Jia, P.-I. Mak, C.-X. Deng and R. P. Martins, *Sci. Rep.*, 2017, **7**, 14586.
- 21 F. Shen, E. K. Davydova, W. Du, J. E. Kreutz, O. Piepenburg and R. F. Ismagilov, *Anal. Chem.*, 2011, **83**, 3533–3540.
- 22 A. Gansen, A. M. Herrick, I. K. Dimov, L. P. Lee and D. T. Chiu, *Lab Chip*, 2012, **12**, 2247–2254.
- 23 B. Sun, F. Shen, S. E. McCalla, J. E. Kreutz, M. A. Karymov and R. F. Ismagilov, *Anal. Chem.*, 2013, **85**, 1540–1546.
- 24 T. D. Rane, L. Chen, H. C. Zec and T.-H. Wang, *Lab Chip*, 2015, **15**, 776–782.
- 25 D. T. Le and N. T. Vu, *Appl. Biol. Chem.*, 2017, **60**, 169–180.
- 26 A. E. Calvert, B. J. Biggerstaff, N. A. Tanner, M. Lauterbach and R. S. Lanciotti, *PLoS One*, 2017, **12**, e0185340.
- 27 D.-K. Kang, M. M. Ali, K. Zhang, S. S. Huang, E. Peterson, M. A. Digman, E. Gratton and W. Zhao, *Nat. Commun.*, 2014, **5**(5427), 1–10.
- 28 L. B. Pinheiro, V. A. Coleman, C. M. Hindson, J. Herrmann, B. J. Hindson, S. Bhat and K. R. Emslie, *Anal. Chem.*, 2012, **84**, 1003–1011.
- 29 X. Wang, Y. Piao, Y. Su and W. Wang, *Microfluid. Nanofluid.*, 2018, **22**, 129.
- 30 F. Shen, W. Du, J. E. Kreutz, A. Fok and R. F. Ismagilov, *Lab Chip*, 2010, **10**, 2666–2672.
- 31 Y. Men, Y. Fu, Z. Chen, P. A. Sims, W. J. Greenleaf and Y. Huang, *Anal. Chem.*, 2012, **84**, 4262–4266.
- 32 V. R. Yelleswarapu, H.-H. Jeong, S. Yadavali and D. Issadore, *Lab Chip*, 2017, **17**, 1083–1094.
- 33 R. Li, Y. Wang, H. Xu, B. Fei and B. Qin, *Sensors*, 2017, **17**, 2685.
- 34 P. Liao, M. Jiang, Z. Chen, F. Zhang, Y. Sun, J. Nie, M. Du, J. Wang, P. Fei and Y. Huang, *Proc. Natl. Acad. Sci. U. S. A.*, 2020, **117**(41), 25628–25633.
- 35 Z. Chen, P. Liao, F. Zhang, M. Jiang, Y. Zhu and Y. Huang, *Lab Chip*, 2017, **17**, 235–240.
- 36 Y. Fu, F. Zhang, X. Zhang, J. Yin, M. Du, M. Jiang, L. Liu, J. Li, Y. Huang and J. Wang, *Commun. Biol.*, 2019, **2**, 147.
- 37 F. Zhang, P. Liao, Y. Sun, Z. Chen, Y. Pang and Y. Huang, *Lab Chip*, 2020, **20**, 2328–2333.
- 38 L. Cao, X. Cui, J. Hu, Z. Li, J. R. Choi, Q. Yang, M. Lin, L. Y. Hui and F. Xu, *Biosens. Bioelectron.*, 2017, **90**, 459–474.
- 39 H. Yuan, Y. Chao and H. C. Shum, *Small*, 2020, **16**(9), 1904469.
- 40 T. Gou, J. Hu, W. Wu, X. Ding, S. Zhou, W. Fang and Y. Mu, *Biosens. Bioelectron.*, 2018, **120**, 144–152.
- 41 F. Hu, J. Li, Z. Zhang, M. Li, S. Zhao, Z. Li and N. Peng, *Anal. Chem.*, 2019, **92**, 2258–2265.
- 42 V. Yelleswarapu, J. R. Buser, M. Haber, J. Baron, E. Inapuri and D. Issadore, *Proc. Natl. Acad. Sci. U. S. A.*, 2019, **116**, 4489–4495.